



Research Paper

Surface plasmon resonance-enhanced solar-driven photocatalytic performance from Ag nanoparticle-decorated self-floating porous black TiO₂ foams

Haoze Li, Liyan Shen, Kaifu Zhang, Bojing Sun, Liping Ren, Panzhe Qiao, Kai Pan, Lei Wang, Wei Zhou*

Key Laboratory of Functional Inorganic Material Chemistry, Ministry of Education of the People's Republic of China, Heilongjiang University, Harbin 150080, PR China



ARTICLE INFO

Article history:

Received 3 July 2017

Received in revised form 3 August 2017

Accepted 6 August 2017

Available online 12 August 2017

Keywords:

Photocatalysis

Black TiO₂

Ag nanoparticle

Self-floating porous foam

Surface plasmon resonance

ABSTRACT

Ag nanoparticle-decorated self-floating porous black TiO₂ foams (Ag-FBTFs) are fabricated by facile wet-impregnation and high-temperature surface hydrogenation strategy, utilizing self-floating porous black TiO₂ foams (FBTFs) with 3D macro-mesoporous architectures as hosts. The composites are evidently investigated by X-ray diffraction (XRD), Raman, N₂ adsorption, diffuse reflectance spectroscopy (DRS), transmission electron microscope (TEM), scanning electron microscopy (SEM), scanning Kelvin Probe (SKP), surface photovoltage spectroscopy (SPS) and photoluminescence (PL). The results show that the small Ag nanoparticles with diameter of 3–4 nm are decorated on the surface of FBTFs uniformly, which extend the photoresponse to visible-light region and show obvious surface plasmon resonance (SPR). The Ag-FBTFs exhibit excellent solar-driven photocatalytic performance for complete mineralization of some high-toxic organic contaminants. The enhancement can be attributed to the 3D macro-mesoporous networks facilitating the diffusion of reactants and products, the floating feature and small Ag nanoparticle-decoration favoring light-harvesting and spatial separation of photogenerated electron-hole pairs due to SPR effect. This novel SPR-enhanced solar-driven floating photocatalyst will have potential application in fields of natural environment.

© 2017 Elsevier B.V. All rights reserved.

1. Introduction

As is known, the environmental pollution and energy shortage have become two key global issues with the development of industry [1–3]. For the sustainable development of society, solving environmental pollution issue and developing environmentally friendly energy have become urgent task [4–7]. In recent years, semiconductor photocatalysis has been regarded as a promising technology due to its widespread application in solving environmental and energy issues [8–15]. Titanium dioxide (TiO₂) is the most representative material for photocatalysis, owing to its chemical stability, non-toxic, high photoelectric conversion efficiency, low-cost and high photocatalytic activity. Nevertheless, anatase TiO₂ with wide band gap of ~3.2 eV can only absorb the UV light, which is ~5% of the sunlight [16–20]. In order to use sunlight effectively, much effort has been made to enhance the light absorp-

tion of TiO₂. Chen and coworkers presented the black TiO₂ with a narrow bandgap through hydrogenation [21]. Compared to traditional white TiO₂, the black TiO₂ nanoparticles improved the solar absorption and photocatalytic activity greatly. Although the discovery of black TiO₂ greatly broadens the light absorption region and increases the utilization ratio of visible light, the high recombination of photogenerated electron-hole pairs still results in poor photocatalytic performance [22–27].

There is no denying that noble metals with surface plasmon resonance (SPR) effect can greatly improve the utilization efficiency of sunlight by extend the optical absorption region [28–32]. Our group synthesized well-ordered mesoporous TiO₂/Ag composite with small Ag clusters confined within the channels of well-ordered mesoporous TiO₂. The Ag clusters could extend the photoresponse to visible light region and increase the separation of photogenerated electron-hole pairs, owing to the strong SPR of Ag clusters [33,34]. The photocatalytic performance of TiO₂/Ag composite was improved significantly. However, the difficulty in separation and recycling of traditional photocatalytic materials limits their practical applications greatly. In the past decade, researchers made

* Corresponding author.

E-mail address: zwchem@hotmail.com (W. Zhou).

much effort to overcome the separation and recycling problem of photocatalytic materials. Fortunately, the emergence of floating photocatalytic materials had successfully solved the above issues, which could float on the water and greatly increased the utilization of sunlight [35–37]. Since then, a large number of floating photocatalysts were synthesized on the floating carriers, such as expanded perlite, natural porous pumice, low density polyethylene (LDPE), etc [38,39]. Nevertheless, it still remained some unsolved issues, including the effective loading, the steadiness on the carriers, and restricting light transmission. Fortunately, the freeze-drying method combined with cast molding technology, followed by a high-temperature surface hydrogenation to synthesize self-floating black TiO₂ foams could solve these above issues [40,41]. However, the solar-driven photocatalytic performance of single-component TiO₂ photocatalyst is still undesirable. Therefore, it is still a great challenge for fabricating floating photocatalytic materials which could satisfy with the separation and recycle, and excellent solar-driven photocatalytic performance simultaneously. Introducing noble metal such as Ag nanoparticles with SPR effect on self-floating black TiO₂ foams would be good candidate for further improving the solar-driven photocatalytic performance.

In this paper, we demonstrate the facile synthesis of Ag nanoparticle-decorated self-floating porous black TiO₂ foams (Ag-FBTFs) by wet-impregnation and high-temperature hydrogen reduction method. The Ag-FBTFs with excellent solar-driven photocatalytic performance can extend the light absorption to visible light region, enhance the diffusion capacity and increase the separation efficiency of photogenerated electron-hole pairs. Moreover, the complete mineralization of some high-toxic organic contaminants by Ag-FBTFs is also studied under AM 1.5 irradiation. Therefore, the novel light-weight Ag-FBTFs which can float on the water and possess SPR effect maybe have really practical applications in environment.

2. Experimental section

2.1. Chemicals

Titanyl sulfate (TiOSO₄), ethanediamine (C₂H₈N₂), ethanol (C₂H₆O), polyacrylamide (C_{3x}H_{5x}N_xO_x) and silver nitrate (AgNO₃) were of analytical grade and purchased from Aladdin Reagent Corp. All chemicals were used as received without any further purification. Deionized water was used for all experiments.

2.2. Synthesis

The synthesis of FBTFs was described elsewhere according to our previous study [40]. The Ag-FBTFs were fabricated by wet-impregnation and high-temperature surface hydrogenation approach. Typically, the FBTFs was added to various concentrations of AgNO₃ solutions for 5 min and dried at 60 °C for 30 min in air atmosphere. Then, the resulted samples were calcined in a quartz reactor for 2 h at 500 °C under hydrogen atmosphere with a constant flow rate (100 mL min⁻¹). The contents of Ag in FBTFs were about 0.5, 1, 2, 3, 4, and 5 wt.%, as measured by inductively coupled plasma optical emission spectrometry (ICP-OES) on an Optima 7000DV (Perkin-Elmer Corp.) instrument.

2.3. Characterization

The Ag-FBTFs were characterized by a wide-angle X-ray diffraction over the diffraction angle range (2θ) 5–80° with a Bruker-Norius D8 advanced diffractometer, using a CuKα ($\lambda = 1.5406 \text{ \AA}$) radiation source operated at 40 kV and 40 mA. The transmission electron microscopy (TEM) images were conducted on a JOEL JEM 2100F operated at 200 kV. Scanning electron

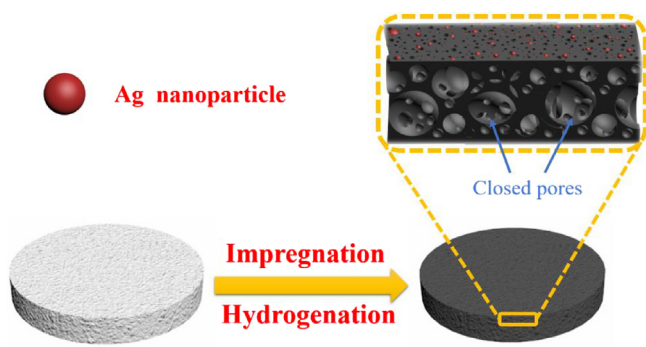
microscope (SEM) images were obtained from a Hitachi S-4800 instrument working at 15 kV. Diffuse reflectance spectroscopy (DRS) was conducted on a UV-vis spectrophotometer (Lambda 950 (PerkinElmer, USA)) in the range of 200–800 nm. Nitrogen adsorption-desorption isotherms at 77 K were collected on an AUTOSORB-1 (Quantachrome Instruments) nitrogen adsorption apparatus. All samples were degassed under vacuum at 180 °C for at least 8 h prior to the measurement. The Brunauer–Emmett–Teller (BET) equation was used to calculate the specific surface area. Pore size distributions were obtained using the Barrett–Joyner–Halenda (BJH) method from the adsorption branch of the isotherms. The total organic carbon (TOC) removal was measured using the TOC analysis equipped with analytic jena multi NIC 2100 analyzer. Surface photovoltage spectroscopy (SPS) measurements were carried out with a home-built apparatus equipped with a lock-in amplifier (SR830) synchronized with a light chopper (SR540). The photoluminescence (PL) spectra were measured by a PE LS 55 spectrofluoro-photometer with excitation wavelength of 332 nm.

2.4. Photocatalytic activity

The photocatalytic activity was evaluated by mineralization of different organic pollutants, such as thiobencarb, atrazine, phenol and octane. The samples were added to above-mentioned solution (40 mL, 1 mg L⁻¹) in weighing bottle without stirring for 1 h in the dark in order to reach an adsorption-desorption equilibrium. The suspension was irradiated by using a 300 W Xe lamp (Autolight CEL-HXF300, 100 mW cm⁻²) with AM 1.5 filter as light source. All photocatalytic experiments were carried out in an open photoreactor located at 15 cm away from the light source without stirring at constant temperature 40 °C. The mineralization of pollutants before and after irradiation was tested by total organic carbon analysis. The single-wavelength efficiency was irradiated with a 300 W Xe lamp with a bandpass filter (365 and 520 nm) system. Photoelectrochemical properties were investigated using a Princeton Versa STAT 3 in a standard three electrode configurations with Ag-FBTFs and FBTFs materials used as photoanodes, Pt foil as the counter electrode, and an Ag/AgCl electrode as the reference electrode. The photoanodes were prepared by a traditional spray coating method, using a glass rod to roll a paste containing 0.2 g of powders and 0.5 mL of EtOH on a transparent conducting glass (TCO, fluorine doped SnO₂ layer, 20 Ω per square, Nippon sheet glass, Japan), and pressed at 1000 kg cm⁻² between stainless-steel plates in a hydraulic press using aluminium foil to prevent adhesion to form a film (2 × 1 cm), followed by calcination at 350 °C under a N₂ atmosphere with a constant heating rate of 10 °C min⁻¹. 1 M KOH purged with N₂ was used as the electrolyte. An AM 1.5 solar power system (Oriel, USA) was used as the light irradiation source.

3. Results and discussion

In this study, we demonstrate the fabrication of Ag nanoparticle-decorated self-floating porous black TiO₂ foams via facile wet-impregnation and high-temperature surface hydrogenation strategy, utilizing self-floating porous black TiO₂ foams with 3D macro-mesoporous architectures as hosts. The illustrated formation process of Ag-FBTFs is shown in **Scheme 1**. Although quantities of large closed pores are formed due to the removal of template under the special conditions of freeze-drying process, there are still many open pores on the surface, which favors the efficient loading of Ag nanoparticles. After wet-impregnation, the Ag ions diffused to these open pores and Ag nanoparticles are formed after hydrogen atmosphere reduction. Due to the confinement effect of the open pores, these Ag nanoparticles are small and uniform, which increase the utilization ration of noble metal greatly. Finally, the



Scheme 1. Schematic illustrating the formation process of Ag-FBTFs.

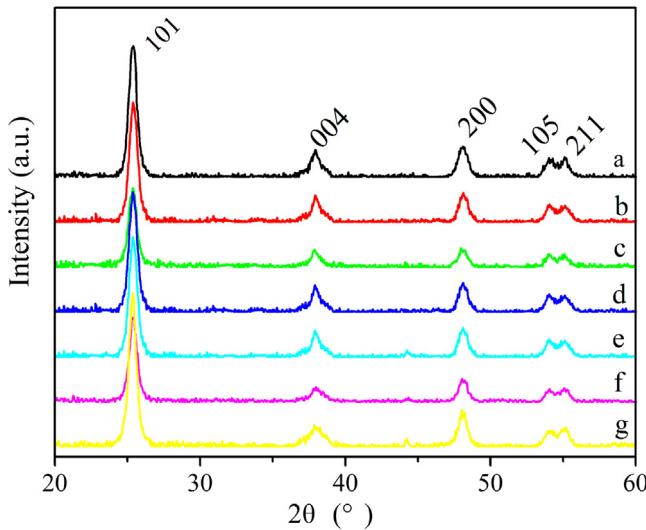


Fig. 1. X-ray diffraction patterns of the FBTFs (a) and Ag-FBTFs with different Ag contents of 0.5 (b), 1 (c), 2 (d), 3 (e), 4 (f), and 5 wt.% (g), respectively.

formed Ag-FBTFs could still float on the water, which could harvest the solar light efficiently.

Fig. 1 shows the typical XRD patterns of the FBTFs (a) and Ag-FBTFs with different Ag contents of 0.5 (b), 1 (c), 2 (d), 3 (e), 4 (f), and 5 wt.% (g), respectively. Five peaks at $2\theta = 25.2, 37.8, 48.1, 53.9$ and 56.1° can be observed, which are ascribed to (101), (004), (200), (105) and (211) planes of anatase TiO₂ (JCPDS, No.21-1272). No other peaks are found, indicating the high purity of the products [42,43]. It should be noted that a typical diffraction peak at

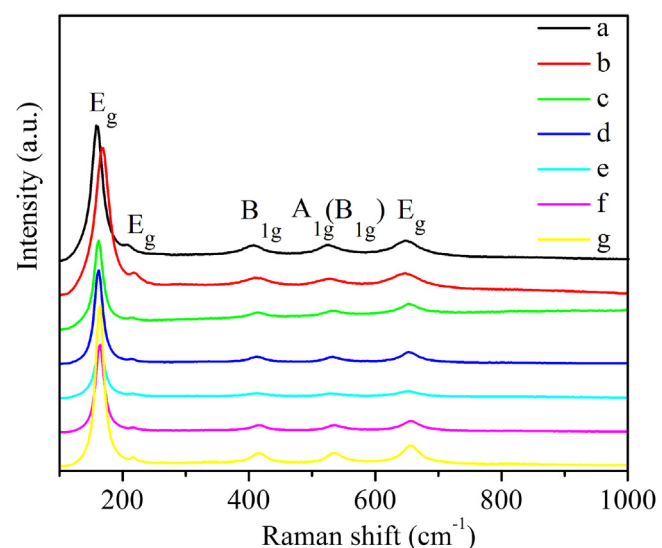


Fig. 2. Raman spectra of the FBTFs (a) and Ag-FBTFs with different Ag contents of 0.5 (b), 1 (c), 2 (d), 3 (e), 4 (f), and 5 wt.% (g), respectively.

$2\theta = 44^\circ$ for Ag appears in Ag-FBTFs composites. The characteristic diffraction peak of Ag increases with the increased content from Fig. 1b-f, confirming the successful fabrication of Ag/TiO₂ composites [33,34].

Fig. 2 shows five Raman vibration peaks at approximately 149, 199, 393, 513, and 639 cm⁻¹ could be attributed to typical anatase TiO₂ Raman bands of E_g , E_g , B_{1g} , A_{1g} (B_{1g}), and E_g modes, respectively [16,17]. The result is in good consistent with the XRD results. Moreover, the main peaks of TiO₂ samples with different contents of Ag particles have a certain blue shift, which is due to the existence of nano-silver. The results demonstrate the successful synthesis of Ag/TiO₂ composites.

The N₂ adsorption-desorption isotherms (A) and the corresponding pore-size distribution curves (B) of the FBTFs (a) and Ag-FBTFs with different Ag contents of 0.5 (b), 1 (c), 2 (d), 3 (e), 4 (f), and 5 wt.% (g), respectively, are shown in Fig. 3. The N₂ adsorption-desorption isotherms are of type-IV curves with a hysteresis loop, indicating the existence of mesoporous structure [40]. The BET surface area of the FBTFs is $\sim 37 \text{ m}^2 \text{ g}^{-1}$. When TiO₂ foams are decorated with Ag nanoparticles, the BET surface areas of Ag-FBTFs are decreased with the increasing Ag contents, which confirm the efficient loading of Ag nanoparticles on floating TiO₂ foams. The appropriate specific surface area and silver loading are beneficial

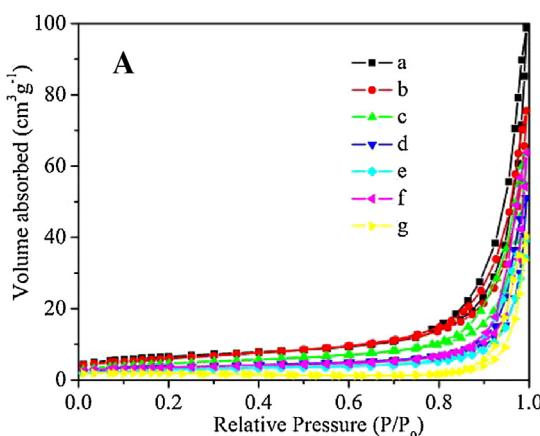


Fig. 3. N₂ adsorption-desorption isotherms (A) and pore-size distribution curves (B) of the FBTFs (a) and Ag-FBTFs with different Ag contents of 0.5 (b), 1 (c), 2 (d), 3 (e), 4 (f), and 5 wt.% (g), respectively.

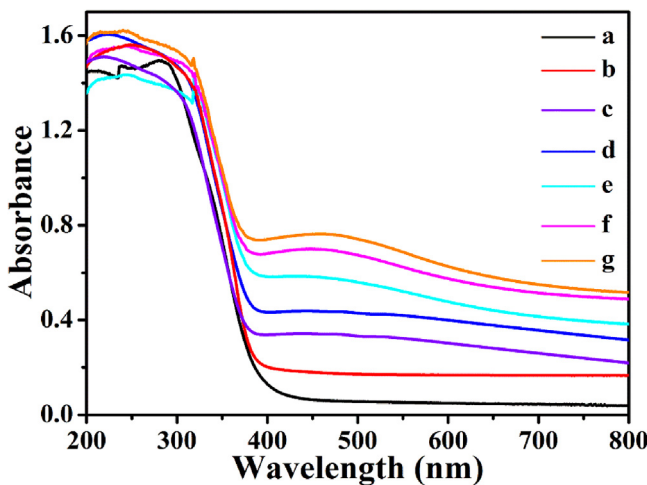


Fig. 4. The ultraviolet-visible absorption spectra of the FBTFs (a) and Ag-FBTFs with different Ag contents of 0.5 (b), 1 (c), 2 (d), 3 (e), 4 (f), and 5 wt.% (g), respectively.

to produce more reaction active sites, which can facilitate the photocatalytic reactions. The pore-size distributions of all samples with different Ag contents are shown in Fig. 3B. It should be noted that the pore sizes are mainly distributed in 30–50 nm, and the pore volumes decrease obviously, indicating the efficient decoration of Ag nanoparticles.

Fig. 4 shows the ultraviolet-visible absorption spectra of the FBTFs (a) and Ag-FBTFs with different Ag contents of 0.5 (b), 1 (c), 2 (d), 3 (e), 4 (f), and 5 wt.% (g), respectively. It clearly indicates that all of the products have strong absorption from ultraviolet to visible light region. In addition, the Ag-FBTFs with different contents of Ag nanoparticles both have a relatively obvious absorption peak at ~ 500 nm, which is ascribed to the SPR of Ag nanoparticles. Obviously, the SPR absorption (400–800 nm) of Ag-FBTFs are obviously increased with increasing supported amounts of Ag nanoparticles. Based on the SPR effect, the light absorption for Ag-FBTFs can be extended to the visible light region [28–30]. We can clearly see that the absorption range of Ag-FBTFs is significantly stronger than that of FBTFs, which is due to the synergistic effect of hydrogenation and SPR effect.

In order to deeply investigate the microstructure of the sample, the Ag-FBTFs with Ag of 3 wt.% (e) is studied by scanning electron microscope (SEM) and transmission electron microscopy (TEM). Fig. 5A shows that the surface of the sample is composed of particles with uniform size. Fig. 5B is the partial magnification, which can be clearly shown macroporous and mesoporous architectures. The presence of the porous structure can shorten the relative migration distance to the surface of the photogenerated charge carriers, resulting in more reactive sites on the surface of the sample, greatly improving the photocatalytic performance. Nevertheless, the Ag nanoparticles are not clearly observed from SEM observation, due to the quite small size. Fig. 5C and D is the TEM images of the sample. As shown in Fig. 5C, the uniform Ag nanoparticles with diameters of about 3–4 nm are successfully loaded on black TiO₂ foams. In addition, Fig. 5D shows that enlarged Ag nanoparticles and the clear lattice stripes confirm that the Ag-FBTFs are highly crystallized. And the lattice fringe spacing is estimated to be ~ 0.35 nm, corresponding to the (101) crystal plane of anatase TiO₂, which is consistent with the XRD results. In addition, the thin amorphous layers are formed at the edge of the black TiO₂, due to the efficient surface hydrogenation.

As high-toxic organic contaminants, Atrazine is chosen for evaluating the photocatalytic performance for Ag-FBTFs. The loading amounts of Ag nanoparticles play vital roles on photocatalytic performance. As shown in Table 1, the photocatalytic performance

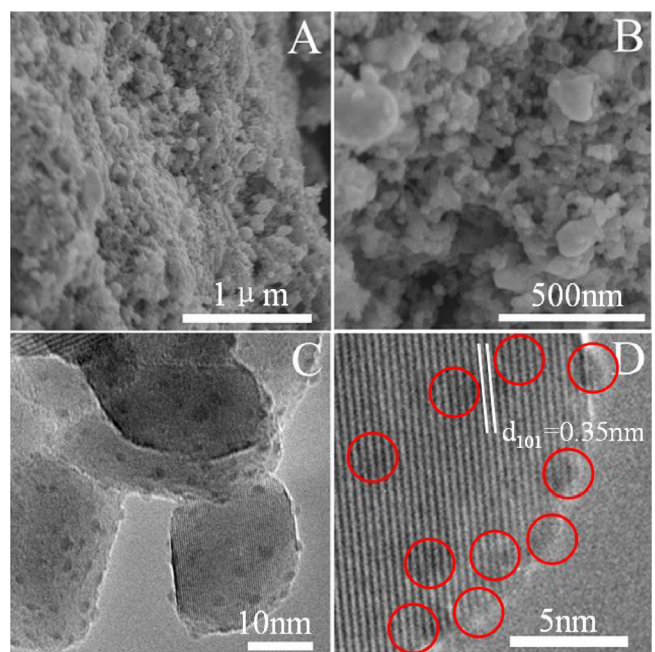


Fig. 5. SEM images (A, B) and TEM images (C, D) of Ag-FBTFs with Ag content of 3 wt.%.

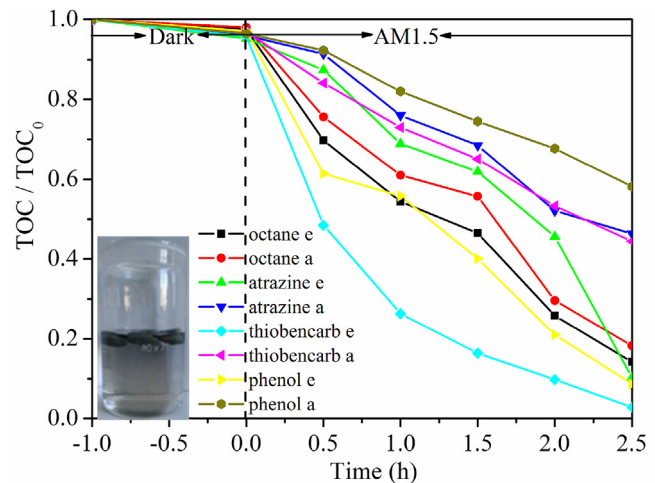


Fig. 6. The TOC removal of four kinds of pollutants under AM 1.5 without stirring for the FBTFs (a) and Ag-FBTFs with different Ag contents of 0.5 (b), 1 (c), 2 (d), 3 (e), 4 (f), and 5 wt.% (g), respectively. The inset is the photo of Ag-FBTFs floating on water.

for Ag-FBTFs containing 3 wt.% Ag nanoparticles is the best one. At the beginning, the photocatalytic performance of Ag-FBTFs is increasing with increasing the Ag loading amount. However, when the amounts of Ag nanoparticles beyond 3 wt.%, the photocatalytic performance decrease with further increasing the loading amount. The results show that high loading amounts will cause aggregation of Ag nanoparticles into large ones (as shown in Fig. S1), decreasing the photocatalytic performance. Therefore, the suitable loading amount of Ag nanoparticles is important for photocatalytic performance.

In order to further evaluate the effect of Ag-FBTFs on the photocatalytic degradation characteristic, the photodegradation of other organic pollutants under AM 1.5 was carried out. Four kinds of organic pollutants, octane, atrazine, thiobencarb and phenol, are chosen as aim contaminants. As can be seen from Fig. 6, the photocatalytic performance of Ag-FBTFs is better than that of FBTFs.

Table 1

The photodegradation ratio of atrazine for Ag-FBTFs with different Ag contents.

Ag content of Ag-FBTFs	0 wt%	0.5 wt%	1 wt%	2 wt%	3 wt%	4 wt%	5 wt%
Photodegradation ratio of atrazine	24%	49.5%	46%	51.3%	62.4%	54.7%	56.3%

It is worthwhile mentioning that the photocatalytic degradation of thiobencarb can be up to 98% in 2.5 h for Ag-FBTFs composite (3 wt.%). The results suggest that Ag-FBTFs possess excellent photocatalytic performance. Although the specific surface area of Ag-FBTFs is less than that of FBTFs, it is beneficial to the diffusion and separation of photogenerated electron-hole pairs due to the SPR effect of Ag nanoparticles. The Ag-FBTFs can provide a large number of active sites due to the presence of heterojunction and the SPR effect of Ag nanoparticles, which can enhance the visible-light-driven photocatalytic performance greatly. Thus, the photocatalytic performance of Ag-FBTFs is better than that of FBTFs. In addition, from Fig. S2, the Ag-FBTFs and FBTFs both show excellent photocatalytic degradation property under 365 nm irradiation, implying the high utilization ratio of UV region for both of them. The photocatalytic performance decreases sharply under single wavelength of 520 nm, confirming the main contribution is still UV light. It is worth noting that the photocatalytic performance for Ag-FBTFs is better than that of FBTFs under 520 nm due to the SPR effect. It is about 3 times higher for Ag-FBTFs than that of FBTFs for 520 nm. The results confirm that the utilization ratio of solar light and the separation efficiency of photogenerated electron-hole pairs are indeed improved significantly due to the SPR effect of Ag nanoparticles. The stability is important for recycling the photocatalyst. The floating Ag-FBTFs can be easily taken out from the solution and recycled. After photocatalysis and recycle for 10 times, the degradation ratio for thiobencarb nearly keeps constant from Fig. 7, further indicating the high stability of Ag-FBTFs and favoring the practical applications in environment.

The scanning Kelvin probe (SKP) is sensitive to discern subtle molecular interactions via vibrating electromagnetic and acoustic fields, which shows a relative flat potential change according to the work function [44]. Fig. 8 shows the SKP microscopy for FBTFs and Ag-FBTFs with different Ag contents. As can be seen from Fig. 7, the measured work functions of a, b, c, d, e, f and g are 5.33, 5.21, 5.19, 5.17, 4.96, 5.07 and 5.16 eV, respectively. It should be pointed out

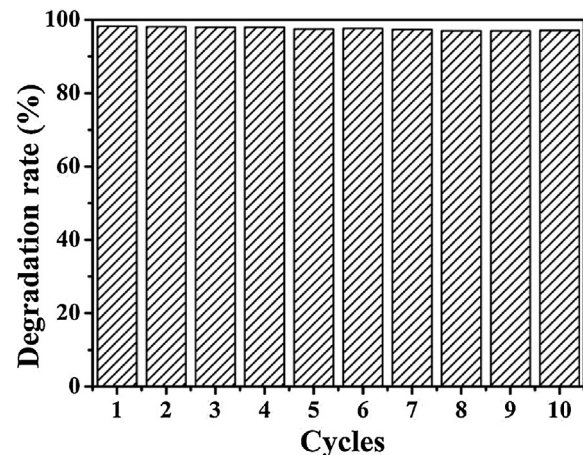


Fig. 7. The recycle of Ag-FBTFs with Ag contents of 3 wt.% for photodegradation of thiobencarb.

that the Ag-FBTFs with Ag content of 3 wt.% has the lowest work function. The low value of the work function indicates the easy escape of photogenerated electrons and then enhances the separation efficiency of photogenerated charge carriers. Thus, it confirms that the Ag-FBTFs with Ag content of 3 wt.% possess the highest photogenerated electron-hole separation efficiency. The approximate Fermi levels for Ag-FBTFs are higher than that of FBTFs, which enhance the built-in electric field and surface band bending, and thus favor the efficient spatial separation of photogenerated electron-hole pairs [45]. Therefore, the solar-driven photocatalytic performance for Ag-FBTFs is better than that of FBTFs.

Fluorescence spectra and surface photovoltage spectroscopy (SPS) are performed to investigate the efficient separation of photogenerated charge carriers. As is known that the efficiency of photogenerated electron-holes probably increase as the flu-

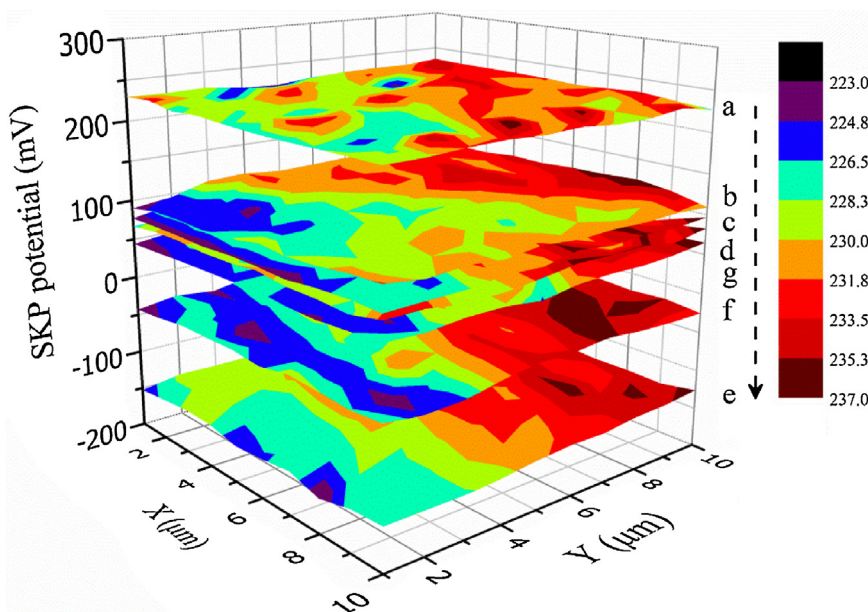


Fig. 8. Kelvin probe microscopic spectra of the FBTFs (a) and Ag-FBTFs with different Ag contents of 0.5 (b), 1 (c), 2 (d), 3 (e), 4 (f), and 5 wt.% (g), respectively.

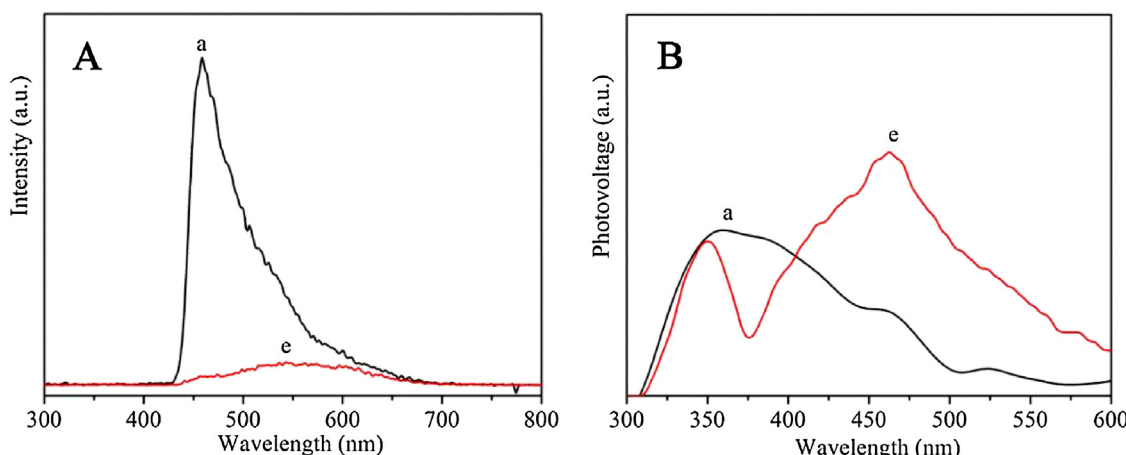


Fig. 9. Fluorescence spectra (A) and surface photovoltage spectra (B) of FBTFs (a) and Ag-FBTFs with Ag content of 3 wt.% (e).

rescence intensity decreases. As can be seen from Fig. 9A, the fluorescence intensity of Ag-FBTFs with Ag content of 3 wt.% (e) is obvious lower than that of FBTFs (a), indicating the low recombination of photogenerated electron-hole pairs for Ag-FBTFs and it is conducive to enhance photocatalytic performance. As shown in Fig. 9B, both FBTFs (a) and Ag-FBTFs with Ag content of 3 wt.% (e) have strong SPS peaks at around 350 nm, which is ascribed to electron transitions from the valence to conduction band (band-to-band transitions, O_{2p}-Ti_{3d}) [27,46]. It should be pointed out that the Ag-FBTFs have a clearly silver response peak at approximate 475 nm [40]. When the sample is exposed to visible-light irradiation, the electron can be efficiently transferred from the Ag to the conduction band of TiO₂, enhancing the electron-hole transport capacity. Accordingly, we can conclude that the Ag-FBTFs enhance the transmission capacity and separation efficiency of photogenerated electron-hole pairs, and thus improve the solar-driven photocatalytic performance. Moreover, the photoelectrochemical properties of the Ag-FBTFs and FBTFs were also performed and shown in Fig. S3. Linear sweeps voltammogram of the Ag-FBTFs shows a photocurrent density of $\sim 18 \mu\text{A cm}^{-2}$, which is almost three times as high as that of FBTFs materials ($\sim 6 \mu\text{A cm}^{-2}$) in 1 M KOH under AM 1.5 irradiation (Fig. S3A). The chronoamperometry responses of both Ag-FBTFs and FBTFs at 0.6 V are constant (Fig. S3B), indicating their good stabilities. Electrochemical impedance spectroscopy (EIS) was performed to investigate the interface charge separation efficiency for the as-prepared samples under dark and AM 1.5 irradiation. As shown in Fig. S3C, we can clearly see that the Ag-FBTFs show smaller impedance than that of FBTFs both under dark and AM 1.5 irradiation, indicating a more efficient charge separation for the former. The Ag-FBTFs and FBTFs both show a positive slope in the Mott-Schottky plots (as shown in Fig. S3D), demonstrating n-type semiconductor characteristics. From the plots, the Ag-FBTFs show a substantially smaller slope than that of FBTFs, indicating the high electron density for Ag-FBTFs, which is responsible for the high photocatalytic performance.

4. Conclusions

In summary, we demonstrated a facile approach for fabricating Ag nanoparticle-decorated self-floating porous black TiO₂ foams by wet-impregnation method combined with high temperature hydrogen reduction. The Ag nanoparticles were successful decorated the black TiO₂ foams. Owing to the SPR effect of Ag nanoparticles, the photoresponse extended to visible light region obviously and the Ag-FBTFs exhibited excellent solar-driven photocatalytic performance for different high-toxic organic con-

taminants. The enhancement was attributed to the SPR effect of Ag nanoparticles improving the visible light absorption and spatial separation of photogenerated charge carriers, the floating feature enhancing the light harvesting, and the 3D porous networks favoring the mass diffusion. This novel and simple strategy could provide a promising strategy to fabricate other high-performance floating SPR-enhanced photocatalytic materials.

Conflict of interest

The authors declare no competing financial interest.

Acknowledgements

We gratefully acknowledge the support of this research by the National Natural Science Foundation of China (21371053, 51672073), and the University Nursing Program for Young Scholars with Creative Talents in Heilongjiang Province (UNPYST-2015014).

Appendix A. Supplementary data

Supplementary data associated with this article can be found, in the online version, at <http://dx.doi.org/10.1016/j.apcatb.2017.08.023>.

References

- [1] X. Liu, J. Iocozzia, Y. Wang, X. Cui, Y. Chen, S. Zhao, Z. Li, Z. Lin, Energy Environ. Sci. 10 (2017) 402–434.
- [2] D. Chen, H. Zhu, S. Yang, N. Li, Q. Xu, H. Li, J. He, J. Lu, Adv. Mater. 28 (2016) 10443–10458.
- [3] S.A. Matlin, G.M.G. Mehta, H. Hopf, A. Krief, Nat. Chem. 7 (2015) 941–943.
- [4] J. Low, J. Yu, M. Jaroniec, S. Wageh, A. Al-Ghamdi, Adv. Mater. 29 (2017) 1601694.
- [5] Q. Ma, Y. Yu, M. Sindoro, A.G. Fance, R. Wang, H. Zhang, Adv. Mater. 29 (2017) 1605361.
- [6] J. Ge, H. Zhao, H. Zhu, J. Huang, L. Shi, S. Yu, Adv. Mater. 28 (2016) 10459–10490.
- [7] G. Lee, S. Kang, S. Min Won, P. Gutruf, Y. Ra Jeong, J. Koo, S. Lee, J.A. Rogers, J. Sook Ha, Adv. Energy Mater. (2017) 1700157.
- [8] C. Boerighter, U. Aslam, S. Linc, ACS Nano 10 (2016) 6108–6115.
- [9] H. Yu, R. Shi, Y. Zhao, G.I.N. Waterhouse, L. Wu, C. Tung, T. Zhang, Adv. Mater. 28 (2016) 9454–9477.
- [10] C. Tang, L. Liu, Y. Li, Z. Bian, Appl. Catal. B: Environ. 201 (2017) 41–47.
- [11] L. Lin, H. Qu, Y. Zhang, X. Wang, ACS Catal. 6 (2016) 3921–3931.
- [12] Z. Dai, F. Qin, H. Zhao, J. Ding, Y. Liu, R. Chen, ACS Catal. 6 (2016) 3180–3192.
- [13] J. Zhang, J. Wang, P. Chen, Y. Sun, S. Wu, Z. Jia, X. Lu, H. Yu, W. Chen, J. Zhu, G. Xie, R. Yang, D. Shi, X. Xu, J. Xiang, K. Liu, G. Zhang, Adv. Mater. 28 (2016) 1950–1956.
- [14] M. Ge, Q. Li, C. Cao, J. Huang, S. Li, S. Zhang, Z. Chen, K. Zhang, S. Al-Deyab, Y. Lai, Adv. Sci. 4 (2017) 1600152.

- [15] Z. Bian, J. Zhu, H. Li, J. Photochem. Photobiol. C: Photochem. Rev. 28 (2016) 72–86.
- [16] W. Li, Z. Wu, J. Wang, A.A. Elzatahry, D. Zhao, Chem. Mater. 26 (2014) 287–298.
- [17] X. Liu, G. Zhu, X. Wang, X. Yuan, T. Lin, F. Huang, Adv. Energy Mater. 6 (2016) 1600452.
- [18] S. Tiewcharoen, C. Warakulwit, V. Lapeyre, P. Garrigue, L. Fourier, C. Elissalde, S. Buffière, P. Legros, M. Gayot, J. Limtrakul, A. Kuhn, Appl. Catal. B: Environ. 204 (2017) 548–560.
- [19] H. Zhou, Y. Jing, M. Pal, Y. Liu, Y. Liu, J. Wang, F. Zhang, D. Zhao, Nanoscale 9 (2017) 1539–1546.
- [20] Y. Gao, J. Zhu, H. An, P. Yan, B. Huang, R. Chen, F. Fan, C. Li, J. Phys. Chem. Lett. 8 (2017) 1419–1423.
- [21] X. Chen, L. Liu, P.Y. Yu, S.S. Mao, Science 331 (2011) 746–750.
- [22] W. Zhou, W. Li, J. Wang, Y. Qu, Y. Yang, Y. Xie, K. Zhang, L. Wang, H. Fu, D. Zhao, J. Am. Chem. Soc. 136 (2014) 9280–9283.
- [23] W. Hu, W. Zhou, K. Zhang, X. Zhang, L. Wang, B. Jiang, G. Tian, D. Zhao, H. Fu, J. Mater. Chem. A 4 (2016) 7495–7502.
- [24] Z. Lian, W. Wang, G. Li, F. Tian, K.S. Schanze, H. Li, ACS Appl. Mater. Interfaces 9 (2017) 16959–16966.
- [25] K. Zhang, W. Zhou, L. Chi, X. Zhang, W. Hu, B. Jiang, K. Pan, G. Tian, Z. Jiang, ChemSusChem 9 (2016) 2841–2848.
- [26] W. Li, J. Liu, D. Zhao, Nat. Rev. Mater. 1 (2016) 16010.
- [27] W. Zhou, F. Sun, K. Pan, G. Tian, B. Jiang, Z. Ren, C. Tian, H. Fu, Adv. Funct. Mater. 21 (2011) 1922–1930.
- [28] J. Wang, R.A. Ando, P.H.C. Camargo, Angew. Chem. Int. Ed. 127 (2015) 7013–7016.
- [29] Z. Lou, M. Fujitsuka, T. Majima, ACS Nano 10 (2016) 6299–6305.
- [30] T. Hao Tan, J. Scott, Y. Hau Ng, R.A. Taylor, K. Aguey-Zinsou, R. Amal, ACS Catal. 6 (2016) 8021–8029.
- [31] O. Elbanna, S. Kim, M. Fujitsuka, T. Majima, Nano Energy 35 (2017) 1–8.
- [32] L. Martínez, A. Mayoral, M. Espiñeira, E. Roman, F.J. Palomares, Y. Huttel, Nanoscale 9 (2017) 6463–6470.
- [33] W. Zhou, T. Li, J. Wang, Y. Qu, K. Pan, Y. Xie, G. Tian, L. Wang, Z. Ren, B. Jiang, H. Fu, Nano Res. 7 (2014) 731–742.
- [34] Y. Choi, H. Kim, G. Moon, S. Jo, W. Choi, ACS Catal. 6 (2016) 821–828.
- [35] Q. An, Y. Zhang, K. Lv, X. Luan, Q. Zhang, F. Shi, Nanoscale 7 (2015) 4553–4558.
- [36] R. Li, L. Zhang, L. Shi, P. Wang, ACS Nano 11 (2017) 3752–3759.
- [37] D. Chen, H. Zhu, S. Yang, N. Li, Q. Xu, H. Li, J. He, J. Lu, Adv. Mater. 28 (2016) 10443–10458.
- [38] L. Zhou, Y. Tan, J. Wang, W. Xu, Y. Yuan, W. Cai, S. Zhu, J. Zhu, Nat. Photon. 10 (2016) 393–398.
- [39] Y. Wang, L. Zhang, P. Wang, ACS Sustainable Chem. Eng. 4 (2016) 1223–1230.
- [40] K. Zhang, W. Zhou, X. Zhang, B. Sun, L. Wang, K. Pan, B. Jiang, G. Tian, H. Fu, Appl. Catal. B: Environ. 206 (2017) 336–343.
- [41] Z. Xing, W. Zhou, F. Du, Y. Qu, G. Tian, K. Pan, C. Tian, H. Fu, Dalton Trans. 43 (2014) 790–798.
- [42] I. Goncharenko, P. Loubeyre, Nature 435 (2005) 1206–1209.
- [43] D. Yu Usachov, V. Yu Davydov, V.S. Levitskii, V.O. Shevelev, D. Marchenko, B.V. Senkovshiy, O. Yu Vilkov, A.G. Rybkin, L.V. Yashina, E.V. Chulkov, I. Yu Sklyadneva, R. Heid, K. Bohnen, C. Laubschat, D.V. Vyalikh, ACS Nano 11 (2017) 6336–6345.
- [44] X. Shan, U. Patel, S. Wang, R. Iglesias, N. Tao, Science 327 (2010) 1363–1366.
- [45] S.U. Nanayakkara, G. Cohen, C.S. Jiang, M.J. Romero, K. Maturova, M. Al-Jassim, J.V.D. Lagermaat, Y. Rosenwaks, J.M. Luther, Nano Lett. 13 (2013) 1278–1284.
- [46] Q. Qiu, L. Xu, D. Wang, Y. Lin, T. Xie, J. Colloid Interface Sci. 501 (2017) 273–281.